Applied Catalysis B: Environmental 307 (2022) 121209

Contents lists available at ScienceDirect

Applied Catalysis B: Environmental

journal homepage: www.elsevier.com/locate/apcatb

Sustainable biomass upgrading coupled with H_2 generation over in-situ oxidized Co_3O_4 electrocatalysts

Chunlin Chen [a,b,1], Zhenqiang Zhou [a,c,1], Jing Liu [a,c,1], Bin Zhu [a,c], Hualei Hu [a], Yong Yang [a], Guoxin Chen [a], Minrui Gao [d], Jian Zhang [a,b,*]

[a] Ningbo Institute of Materials Technology & Engineering, Chinese Academy of Sciences, 1219 Zhongguan West Road, Ningbo 315201, China
[b] University of Chinese Academy of Sciences, Beijing 100049, China
[c] Nano Science and Technology Institute, University of Science and Technology of China, 166 Renai Road, Suzhou 215123, China
[d] Hefei National Laboratory for Physical Sciences at Microscale University of Science and Technology of China, 96 Jinzhai Road, Hefei 230026, China

ARTICLE INFO

Keywords:
Cobalt oxide
Hydrogen evolution reaction
2
5-bis(hydroxymethyl)furan
2,5-furandicarboxylic acid
Photovoltaic electrocatalysis

ABSTRACT

Substituting overall water splitting with simultaneous biomass upgrading and H_2 evolution has drawn tremendous attention due to the lower energy barrier and higher safety. Developing a cheap, efficient, and durable electrocatalyst with dual function is crucial to this novel coupling system. Herein, we propose the in-situ electrochemical tuning nonporous CoS_x to hydrangea-like Co_3O_4 as a highly effective versatile electrocatalyst for the first time. Due to the defective structures and abundant electroactive sites, the Co_3O_4 catalyst achieved a complete conversion of 5-hydroxymethylfurfural (HMF) to 2,5-furandicarboxylic acid (FDCA) with 93.2% yield and 92.9% faradaic efficiency (FE), as well as a pure hydrogen evolution with 99.8% FE. Interestingly, it harvested a better performance with 95.8% FDCA yield for electro-oxidation of the more stable 2,5-bis(hydroxymethyl)furan (BHMF). Finally, a solar-driven integration reaction was constructed for the first time using the photovoltaic electrocatalysis (PVEC) of BHMF for the efficient and sustainable production of FDCA and H_2.

1. Introduction

Green energy and resources are the essential foundation for the long-term sustainable development of human society. As the ultimate mode of green hydrogen production, overall water splitting (OWS) to hydrogen through electrocatalysis is an efficient and sustainable approach to reducing fossil resource consumption and environmental pollution, contributing to realizing a carbon-balanced energy picture [1]. However, the development of OWS is limited by its anodic half-reaction, i.e., oxygen evolution reaction (OER). Compared to the cathodic hydrogen evolution reaction (HER), OER is a kinetically sluggish process with multiple steps of proton-coupled electron transfer. Since air separation is very mature and cheap, oxygen generated from OER is not highly valuable, depressing the energy efficiency and the economics of the OWS process. Most importantly, the potential crossover of O_2 and H_2 could cause a massive security hazard, thus requiring expensive proton exchange membranes to avoid the risk. To solve these problems, one promising strategy is to substitute OER with thermodynamically favorable reactions, which is beneficial to lowering the energy barrier of anode reaction and consequently accelerating the overall reaction rate [2].

As an alternative oxidation reaction, the conversion of bio-based alcohols and aldehydes into their corresponding aldehydes or acids is conducive to significantly improving the value and expanding the application of natural biomass, which is considered a sustainable energy and substance resource because of its abundance and carbon-neutral features. Among the diverse molecules derived from biomass, furans with hydroxyl and formyl substituents have received increasing attraction because their unique structure allows the production of more value-added chemicals. As the most famous furanic platform chemical, 5-hydroxymethylfurfural (HMF) has been extensively reported to upgrade into the high-value-added 2,5-furandicarboxylic acid (FDCA), which has broad applications in polymers, pharmaceuticals, cosmetics, and other fine chemicals [3,4]. However, the conventional thermal-driven conversion of HMF into FDCA generally required harsh reaction conditions (high temperature and high oxygen pressure) even

* Corresponding author at: Ningbo Institute of Materials Technology & Engineering, Chinese Academy of Sciences, 1219 Zhongguan West Road, Ningbo 315201, China.
E-mail address: jzhang@nimte.ac.cn (J. Zhang).
[1] These authors contributed equally to this work.

https://doi.org/10.1016/j.apcatb.2022.121209
Received 27 October 2021; Received in revised form 27 January 2022; Accepted 10 February 2022
Available online 12 February 2022

in the presence of noble metal catalysts. Compared with thermocatalysis, electrocatalysis possesses many advantages, such as accurate proceeding regulation, mild reaction conditions, broad substrate tolerance, high energy efficiency, and superior operating safety, which shows great potential in the selective oxidation of alcohols and aldehydes by employing a directional flow of electrons as an energy injection mode to drive the oxidation process.

Considering the above aspects, electrochemical oxidation of furans, such as HMF, furfuryl alcohol (FFA), and furfural (FF), was often chosen to substitute the sluggish OER due to their thermodynamically more favorable properties [5]. Moreover, coupling gas-producing HER with furan electro-oxidation reaction (FEOR) in a membrane-free reactor could further elevate energy utilization efficiency and achieve the highly pure hydrogen and value-added oxidation products. In addition, the safety concern in water splitting due to the potential O_2/H_2 crossover can be avoided. Although several noble metals and their corresponding supported catalysts, such as Pt [6], Au [7], Pt/Fe_3O_4/rGO [8], Ir-Co_3O_4 [9], and Pd_1Au_2/C [10], have been applied for FEORs, the situation has been dramatically changed where more thermocatalytically inert materials became active under the driven force of electrochemical potential. Considering the insufficient reserve and high cost of precious metal catalysts, cheap and easily available catalysts developed from earth-abundant elements are undoubtedly more appealing. In the past three decades, researchers made great efforts in exploiting efficient catalysts for FEOR, such as transition metals[11,12] and their oxides [13–18], hydroxides [18–21], nitrides [22,23], sulfides [5], phosphides [24,25], borides [26], selenides [27,28], which were reported to be comparable or superior to noble metal catalysts. Nevertheless, some of the above electrocatalysts were only reported to be active for the single FEOR, whereas designing efficient bifunctional non-precious metal electrocatalysts for simultaneous FEOR and HER is currently more creative and attractive in this field. We recently reported Co_3O_4 nanowires as an excellent bifunctional electrocatalyst for the integrated HMF oxidation and HER [15]. However, the synthesis of nanowires by hydrothermal and subsequent pyrolysis was relatively tedious and time-consuming for industrialization, and the catalytic performance also needs to be improved. Inspired by the promising activity of the cobalt-based catalyst, we attempt to seek much convenient approaches to prepare efficient catalysts. Previous research proved that the sulfides of cobalt are very positive towards both HER and OER in alkaline electrolytes. However, cobalt sulfides are not stable enough during the OER and will finally transform into cobalt oxides or oxyhydroxides [29]. Therefore, in-situ transform the unstable “precatalyst” to a stable and efficient catalyst will open up a new perspective for catalyst preparation.

In this work, we report the growth of the hydrangea-like Co_3O_4 on cobalt foam (Co_3O_4/CF) via sulfuration and in-situ electrochemical oxidation (Scheme 1) as a bifunctional electrocatalyst for integrating FEOR and HER. Owing to its defective structures and abundant active sites, the Co_3O_4/CF achieved a current density of 20 mA·cm^{-2} at the potential of 1.286 V vs. RHE, which is 180 mV lower than that of anodic OER when HMF substituted H_2O as substrate. For the simultaneous HMF oxidation and HER, Co_3O_4/CF needed only 1.385 V to reach the benchmark current density of 10 mA·cm^{-2} in a two-electrode electrolyzer. In the integrated electrolysis at a constant voltage of 1.65 V, HMF completely converted with 93.2% yield and 92.9% Faradaic efficiency (FE) toward the oxidation product FDCA, accompanied by pure hydrogen evolution with 99.8% FE. Remarkably, the micromorphology and catalytic performance of Co_3O_4/CF are almost unchanged after six integration cycles. Furthermore, we demonstrated Co_3O_4/CF with robust FEOR properties by expanding substrates to FFA, FF, 2,5-diformylfuran (DFF), and 2,5-bis(hydroxymethyl)furan (BHMF). Interestingly, though the highly reactive aldehyde group of HMF is reduced to the more stable hydroxyl group, the Co_3O_4/CF harvested a little better performance with 95.82% yield and 95.79% FE for electro-oxidation BHMF into FDCA under the same voltage. Finally, we constructed BHMF-containing photovoltaic electrocatalysis (PVEC) for the first time to demonstrate the concept of utilizing solar energy to drive the coupling reactions and efficiently improve overall sustainability.

2. Materials and methods

2.1. Materials

HMF (> 99.0%) and BHMF (> 99.0%) were supplied by Zhejiang Sugar Energy Technology Co., Ltd (Ningbo, China). Analytical reagent grade sulfur powder, FFA, FF, and DFF, as well as guaranteed reagent grade KOH, ammonium formate, and methanol, were purchased from Aladdin Chemicals Co., Ltd (Shanghai, China). Cobalt foam was purchased from Kunshan Tengerhui Electronic Technology Co., Ltd (Soochow, China). Home-made ultrapure water was used in all experiments.

2.2. Preparation of electrodes

Generally, cobalt foam (CF) with a size of 3 × 0.5 × 0.2 cm was washed in turn with aqueous ethanol, 1.0 M HCl solution, and deionized water for every 10 min under ultrasonic conditions. Then, 4 pieces of cleaned and dried CF were placed in a corundum boat which located in the center of a tube furnace, while 0.5 g sulfur powder was spread in another corundum boat at the upstream side. The tube furnace purged with nitrogen for 30 min, and then heated to 350 °C at a ramping rate of 10 °C min^{-1} and kept for 30 min. The sulfurized sample was noted as CoS_x/CF and then used as a working electrode to conduct a chronopotentiometric oxidation at 10 mA cm^{-2} for 2 h in a 1.0 M KOH electrolyte (without stirring). Finally, the oxidized electrode was cleaned with deionized water, dried at 60 °C for 8 h, and noted as CoO_x/CF.

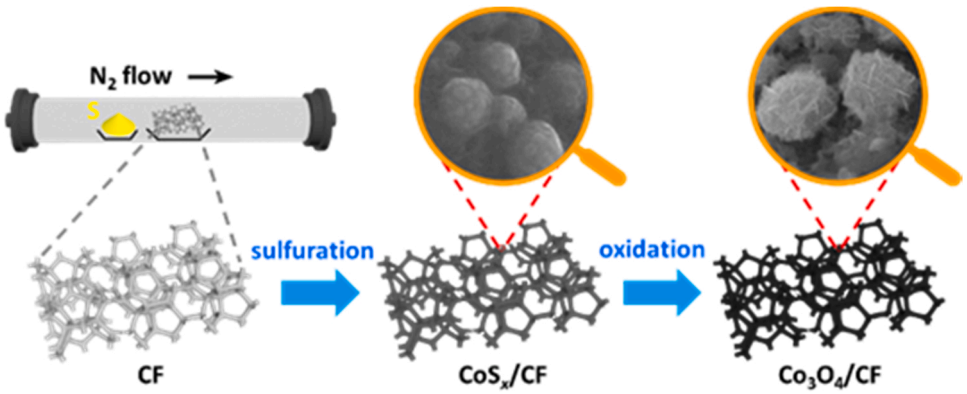

Scheme 1. In-situ fabrication of Co_3O_4/CF via sulfuration and electrochemical activation.

2.3. Characterization

A Bruker D8 DISCOVER X-ray diffraction (XRD) instrument with Cu Kα radiation source was used to analyze the samples' crystal structure. Low magnification morphology was investigated using a Hitachi S4800 scanning electron microscope (SEM) at an acceleration voltage of 8 kV. High magnification morphology and lattice structure were carried out on a high-resolution FEI F20 transmission electron microscope (TEM) equipped with selected area electron diffraction (SAED) at an operating voltage of 200 kV. The surface chemistry of samples was collected through a Shimadzu AXIS UTLTRADLD X-ray photoelectron spectroscopy (XPS) with an Al Kα radiation source.

2.4. Electrochemical experiments and PVEC setup

All the electrochemical experiments were performed at room temperature using a CHI 760E electrochemical analyzer (CH Instruments, Inc, Shanghai.). The standard three-electrode configuration was equipped with a working electrode, an Hg/HgO reference electrode, and a graphite rod counter electrode in an aqueous electrolyte of N_2-saturated 1.0 M KOH solution. All the potentials were calibrated relative to the reversible hydrogen electrode (RHE) potentials by the equation: $E_{RHE} = E_{Hg/HgO} + 0.059 \times pH + 0.098$. In the two-electrode system, two working electrodes were used as cathode and anode in a membrane-free reactor with the same electrolyte. All polarization curves were corrected with 85% iR compensation.

In PVEC, an 0.65 W solar cell battery (80 × 60 mm) was employed to provide the suitable voltage by adjusting the light shade. The estimated photoelectric conversion efficiency was ~13.5%. The sampling tube was inserted into the electrolyte to prevent hydrogen leakage when collecting furan samples for HPLC analysis. The produced hydrogen was collected by the drainage method (detailed in Supporting information). All electrochemical measurements were stirred at 400 rpm by a magnetic stirrer.

2.5. Products analysis

The qualitative and quantitative analysis of furans products was conducted on a high-performance liquid chromatograph (HPLC, Agilent Technologies 1260 II) equipped with a UV dual-wavelength detector and an Agilent Poroshell 120 EC-C18 column set at 40 °C. The wavelengths set at $\lambda = 220$ nm for detection of BHMF, while $\lambda = 265$ nm for detection of HMF, 5-hydroxymethyl-2-furancarboxylic acid (HMFCA), 5-formyl-2-furancarboxylic acid (FFCA), DFF, and FDCA. The mobile phase was 5 mM ammonium formate/methanol (v/v= 3/7) at a flow rate of 5 mL min^{-1}. The conversion of organic substrates and the yield of oxidation products were calculated by Eq. (1) and (2):

$$\text{Conversion}\ (\%) = \frac{\text{mol of organic substrate consumed}}{\text{mol of initial organic substrate}} \times 100\% \quad (1)$$

$$\text{Yield}\ (\%) = \frac{\text{mol of oxidation product detected}}{\text{mol of initial organic substrate}} \times 100\% \quad (2)$$

The faradaic efficiency (FE) towards FDCA or H_2 was obtained by the following Eq. (3):

$$\text{FE}\ (\%) = \frac{\text{mol of product detected} \times n \times F}{\text{total charge passed}} \times 100\% \quad (3)$$

In which n is the number of electrons transferred for FDCA or H_2 formation, F is the Faraday constant (96485 C mol^{-1}), and the total charge passed is the theoretical stoichiometric amount of charge needed to fully convert HMF or BHMF into FDCA, according to the following reaction Eqs. (4–6):

$$HMF + 6\ OH^- \rightarrow FDCA + 4H_2O + 6\ e^-\ n{=}6 \quad (4)$$

$$BHMF + 8\ OH^- \rightarrow FDCA + 4H_2O + 8\ e^-\ n{=}8 \quad (5)$$

$$2H_2O + 2\ e^- \rightarrow 2OH^- + H_2\ n{=}2 \quad (6)$$

3. Results and discussion

3.1. Structural analysis

During the preparation, we noted that the apparent color of CF changed from metallic luster to dark gray by sulfuration and further turned black after electrochemical oxidation. XRD was employed to check the intrinsic structural evolution. To exclude the interference of metal Co substrate, the generated CoS_x on the CF surface was peeled off by ultrasonic (200 W, 4 h, 23 ± 2 °C). As demonstrated in Fig. 1, the XRD pattern of exfoliated CoS_x shows a set of peaks at 16.3, 26.7, 31.5, 38.2, 47.3, 50.3, and 55.1 degrees, which highly matches the (111), (220), (311), (400), (422), (511), and (440) facets of the cubic phase Co_3S_4 (PDF 47–1738), respectively. Besides, there are three weaker diffraction peaks at 29.8, 36.2, 52.1, and 61.2 degrees, assigning to the (311), (400), (440), and (533) facets of the cubic Co_9S_8 (PDF 65–6801), respectively. After electrochemical oxidation, the characteristic diffractions of Co_3S_4 and Co_9S_8 disappeared, while a new set of signals at 19.1, 31.4, 37.0, 38.7, 45.0, 55.9, 59.6, and 65.5 degrees arose, belonging to the (111), (220), (311), (222), (400), (422), (511), and (440) facets of the cubic Co_3O_4 (PDF 65–3103), respectively.

X-ray photoelectron spectroscopy (XPS) measurements reveal that two signals in the region of S *2s* (229 eV) and S *2p* (169 eV) existed in CoS_x/CF but not present in CoO_x/CF (Fig. 2), suggesting the sufficient removal of surface sulfur species by oxidative treatment. Inductively coupled plasma optical emission spectrometry (ICP-OES) tests further verified the substituted S element was penetrated into the electrolyte, showing a concentration of S in the used electrolyte with 107.9 mg kg^{-1} being 125 times that in the blank electrolyte (0.86 mg kg^{-1}). Although previous researches reported the synthesis of CoS_x from Co_3O_4 by anion exchange reaction in sufficient S^{2-} solution at elevated temperature [30], our results undoubtedly demonstrated the facile and complete transformation of CoS_x into Co_3O_4 driven by anode bias and strong alkaline in mild conditions. Based on the above, the growth mechanism of Co_3O_4 can be described as follows.

$$Co_3S_4 + 8OH^- \rightarrow Co_3O_4 + 4S^{2-} + 4H_2O \quad (7)$$

$$Co_9S_8 + 24OH^- \rightarrow 3Co_3O_4 + 8S^{2-} + 12H_2O \quad (8)$$

The surface microstructural aspects were investigated in detail by

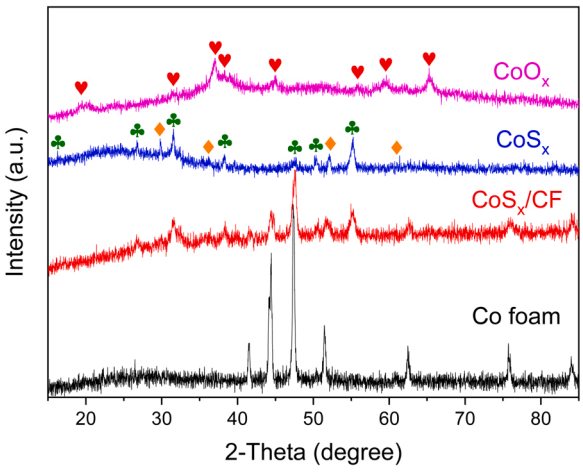

Fig. 1. XRD patterns of exfoliated CoO_x and CoS_x, CoS_x/CF, as well as metal Co foam. Heart: #65-3103 Co_3O_4; club: #47-1738 Co_3S_4; diamond: #65-6801 Co_9S_8.

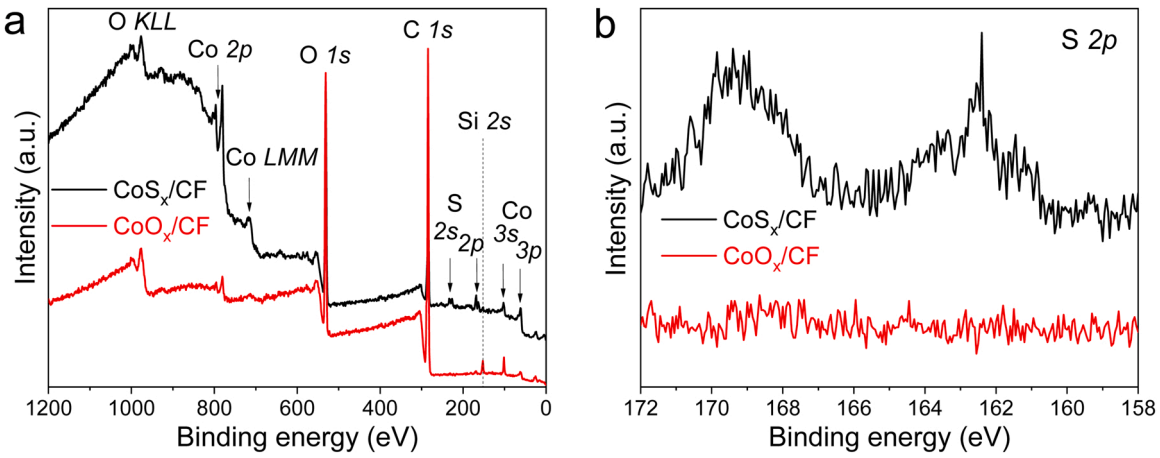

Fig. 2. The XPS results of CoS_x/CF and CoO_x/CF. (a) Survey and (b) S *2p* spectra.

SEM, TEM, and SAED. As depicted in Fig. 3a-c, sulfuration of CF results in a rough surface decorated with microspheres in diameter of 200–400 nm, while the bare CF features a smooth surface (Fig. S1). The TEM image in Fig. 3d reveals that the generated CoS_x microspheres featured a solid structure without apparent pores or channels inside. The high-resolution TEM (HRTEM) image in Fig. 3e exhibits the lattice fringes of 0.284, 0.236, and 0.248 nm, corresponding to the (311) and (440) facets of Co_3S_4 as well as (400) ones of Co_9S_8, respectively. The lattice spacing measurements were double-checked by the fast Fourier transform (FFT) and the inverse FFT operation, as supplemented in Fig. S2&3. The scattered SAED patterns in Fig. 3f proved the refined crystallinity with misoriented grain features, echoing the weaker XRD diffraction. After electrochemical oxidation, the rough surface in large range was well preserved with no cracks, and the microspheres were still anchored on its surface (Fig. 3g). Interestingly, in higher magnification SEM and TEM observations (Fig. 3h&i), each microsphere consists of numerous standing nanosheets on the surface, similar to a bush of hydrangea. The standing structures are contributed to exposing more edges as the active sites, increasing the contact with the reaction media, and promoting the mass transfer, thereby improving the performance for catalysis or energy applications. HRTEM images in Fig. 3j&k further reveal that the oxidized microstructure is highly defective with nanoscale pores, channels, and grain boundaries. With the assistance of FFT and inverse transformation, the lattice fringes of 0.467, 0.287, and 0.246 nm match very well with the (111), (220), (311) planes of Co_3O_4, respectively. The recorded SAED patterns in Fig. 3 display inconsecutive diffraction rings with scattered spots, suggesting a limited crystallinity because the phase transformation was carried out in such a mild and green manner. Indexing of SAED patterns indicates that CoS_x has been completely transformed into pure Co_3O_4. Thus, the previously noted CoO_x/CF can be accurately labeled as Co_3O_4/CF.

3.2. Individual evaluation in a three-electrode cell

The conductive foam decorated with hierarchical and defective microstructure endows Co_3O_4/CF with great application potentials in catalysis, especially in electrochemical catalysis. Directly employing Co_3O_4/CF as a monolithic electrode, it is very convenient to evaluate the catalytic performance of anodic oxidation and cathodic reduction. For anodic reaction, since the OER could compete with FEOR [10], the as-synthesized Co_3O_4/CF and the control sample CF were independently examined as working electrodes in a standard three-electrode cell with and without HMF as the representative furan compound. As shown in Fig. 4a, linear sweep voltammetry (LSV) revealed that the Co_3O_4/CF exhibited a 1.466 V vs. RHE anodic potential at 20 mA cm^{-2} current density in 1.0 M KOH without HMF participation. In contrast, a more positive 1.605 V vs. RHE needed to reach the same current density for the contrast CF. That is, the overpotential is only 236 mV (@ 20 mA cm^{-2}) for OER over Co_3O_4/CF, being much lower than most well-designed electrocatalysts or electrodes (Table S1). It is worth noting that the LSV curve of Co_3O_4/CF appears in the vicinities of 1.15 and 1.35 V vs. RHE with two pre-OER peaks, which were assigned to Co^{2+}→Co^{3+} (initiated at ~0.9 V vs. RHE) and Co^{3+}→Co^{4+} (initiated at ~1.2 V vs. RHE), respectively [18]. After adding 10 mM HMF, the anodic current quickly increased after 0.945 V vs. RHE (onset) and plateaued after 1.1 V vs. RHE, which was attributed to the fact that Co^{3+} could only oxidize the formyl rather than the hydroxyl group of HMF to form HMFCA [18]. When the applied potential was increased to 1.2 V vs. RHE and higher, the generated Co^{4+} could fast oxidize both hydroxyl and formyl groups to achieve a significant anodic current. Therefore, the electrogenerated Co^{3+} and Co^{4+} were considered as the catalytically active sites for HMF oxidation [18,31]. In the presence of HMF, the LSV curves were found to shift toward more negative potentials, suggesting that HMF oxidation is thermodynamically more favorable than OER over both Co_3O_4/CF and CF electrodes. Remarkably, this potential drop of Co_3O_4/CF is particularly pronounced, with a negative shift of more than approximately four times that of CF. The anodic potentials required for HMF oxidation were only 1.079, 1.286, 1.351, and 1.400 V vs. RHE to reach the representative current densities of 10, 20, 50, and 100 mA cm^{-2}, respectively. As far as we know, this performance is superior to that of most reported catalysts towards electrocatalytic HMF oxidation (Table 1&S2). We also note that the result is far better than that of our previously reported Co_3O_4 nanowires catalyst (CoNW/NF) under the same HMF concentration of 10 mM, which required potentials of 1.367, 1.467, and 1.618 V vs. RHE (corrected with 85% iR compensation) to reach 20, 50, and 100 mA cm^{-2}, respectively.

It is well known that metal foam features considerable HER performance due to its excellent conductivity and large accessible surface area. Further surface modification with defective Co_3O_4 structure can provide more active sites to promote the cathodic reaction. As shown in Fig. 4b, Co_3O_4/CF exhibited a steeper LSV curve with a dramatically positive shift, suggesting the hydrogen generation behavior superior to CF in the absence of HMF. Quantitatively, the former required overpotentials of only 177 and 294 mV to attain the benchmark current densities of − 10 and − 100 mA cm^{-2}, respectively, much less than the relative requirements of 275 and 446 mV over CF. The HER overpotential of Co_3O_4/CF is far below that of many reported electrodes, such as NiFe LDH/NF (210 mV at −10 mA cm^{-2}) [32], Ni_3S_2/NF (223 mV at −10 mA cm^{-2}) [33], CoO_x @CN (232 mV at −10 mA cm^{-2}) [34], Co@BCN (183 mV at −10 mA cm^{-2}) [35], α-NiOOH/NF (282 mV at −10 mA cm^{-2}) [36], NiSe nanoflakes (217 mV at −10 mA cm^{-2}) [37], $Co(OH)_2$ @NCNTs@NF (410 mV at −100 mA cm^{-2}) [38], CoO

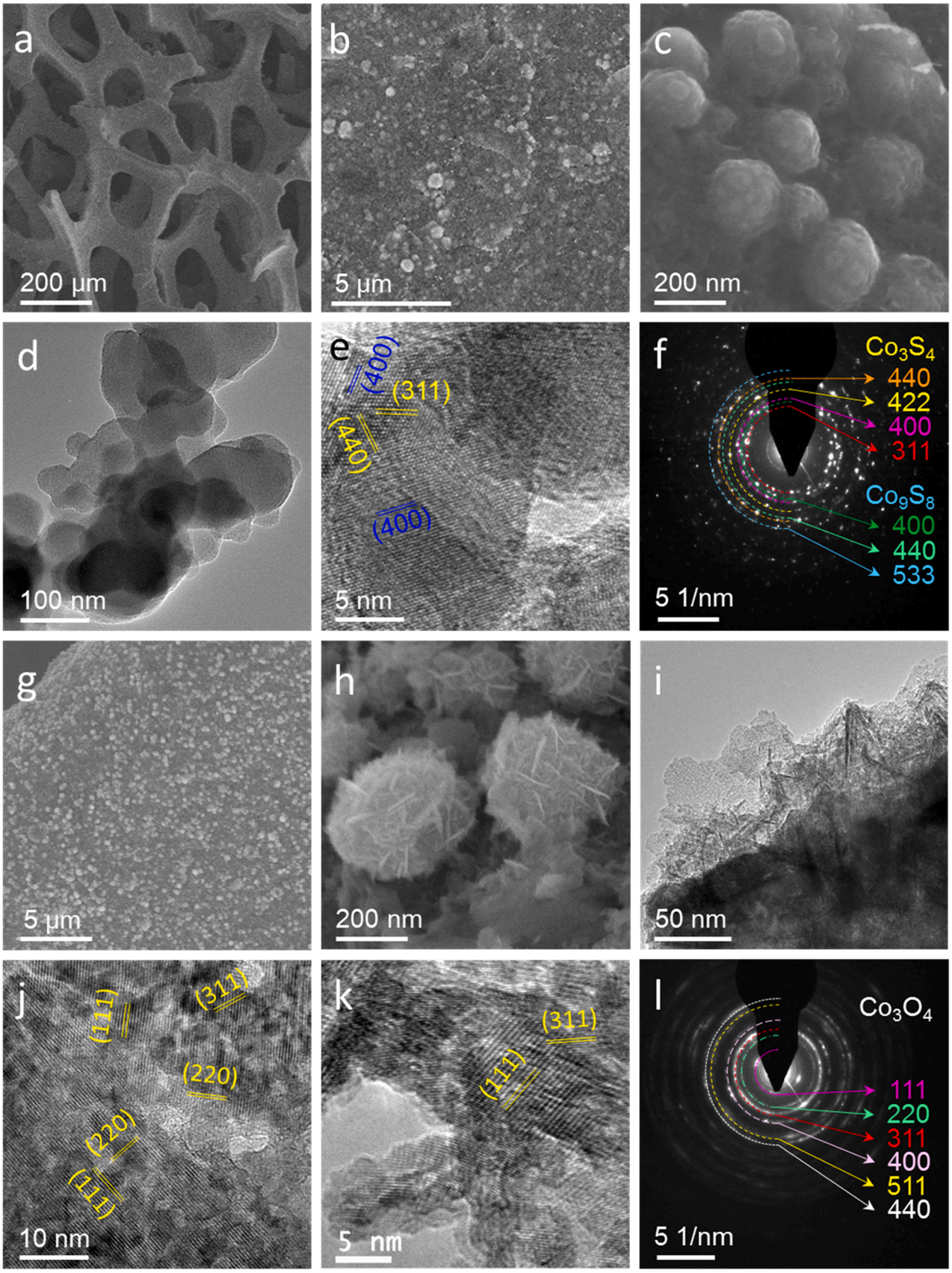

Fig. 3. Electron microscope characterization. (a-c) SEM images of CoS_x/CF. (d-e) TEM images and (f) SAED pattern of exfoliated CoS_x. (g-h) SEM images of CoO_x/CF. (i-k) TEM images and (l) SAED pattern of exfoliated CoO_x.

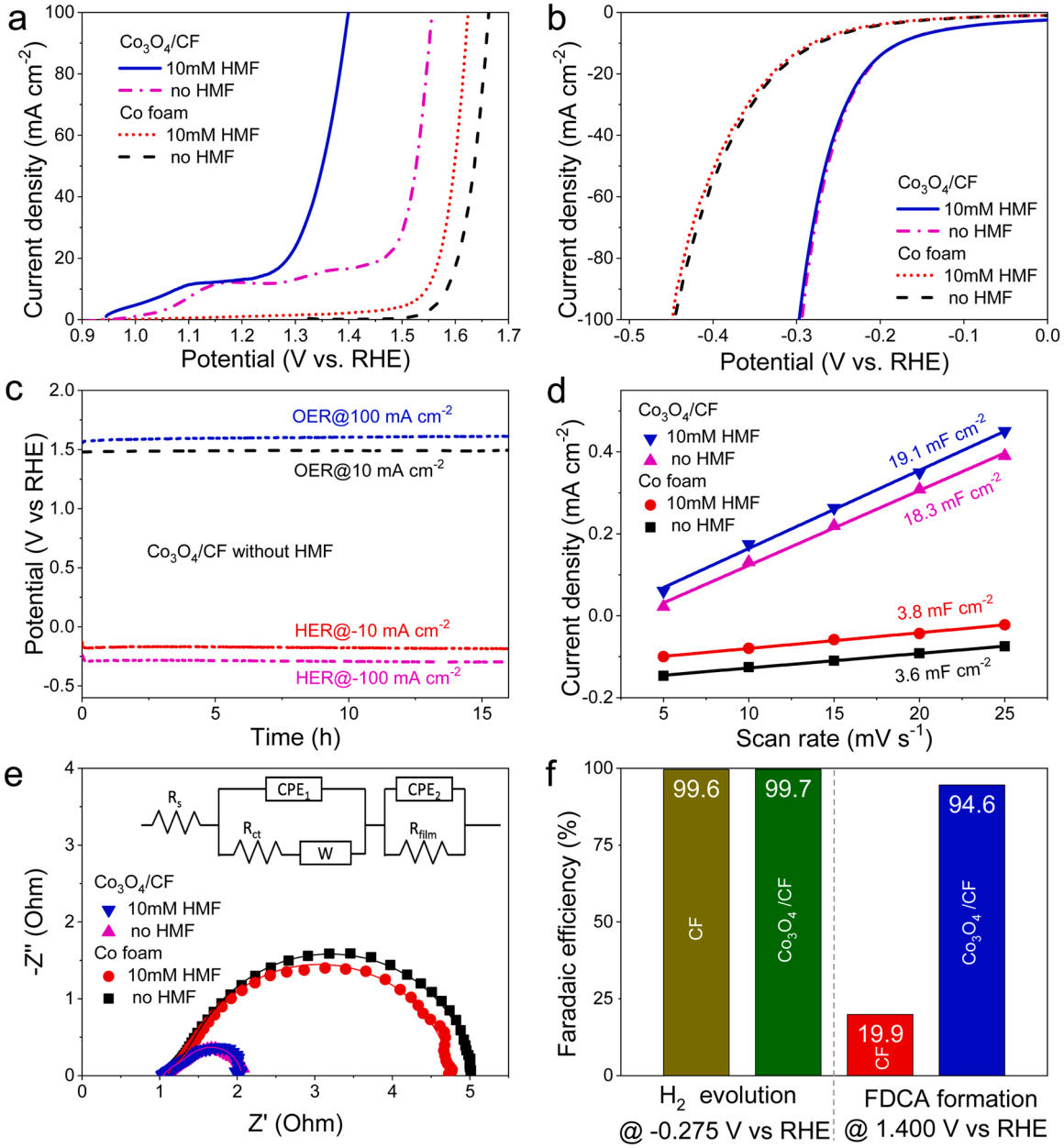

Fig. 4. Electrocatalytic evaluation of individual electrodes in a three-electrode system. (a) Anodic and (b) cathodic LSV curves of Co_3O_4/CF and CF in the absence and presence of HMF. (c) The catalytic stability of Co_3O_4/CF at different current densities. (d) The capacitive current density at 1.018 V vs. RHE as a function of CV scan rate. (e) Nyquist plots of the frequency range from 0.01 Hz to 100 kHz (inset: the fitted equivalent circuit). (f) Faradaic efficiencies for H_2 evolution and FDCA formation.

$(OH)_{0.75}S_{0.25}$ (360 mV at −100 mA cm^{-2}) [39], NiSe@NiO_x (208 mV at −10 mA cm^{-2}) [27], and our previously fabricated CoNW/NF (232 mV at −10 mA cm^{-2}) (detail comparison in Table S3) [15]. From another perspective, by applying the same potential, the current density of Co_3O_4/CF is 3.0–7.7 times that of CF in the range from − 0.177 to − 0.294 V vs. RHE, verifying the great enhancement of electrocatalytic activity toward HER by surface modification again. When HMF joined the electrochemical system, reducing the aldehyde group was possible to compete with HER due to its high reactivity in alkali conditions. However, the polarization curve of Co_3O_4/CF in the presence of HMF is almost impervious with just a tiny negative shift of at most 3 mV at a relatively high current density of − 100 mA cm^{-2}, unambiguously demonstrating the outstanding selectivity of Co_3O_4/CF toward HER and the negligible influence of HMF on cathodic performance. In contrast, the cathodic shifts of potential over CF after HMF participation are slightly increased to 8 mV at the current density of − 5 mA cm^{-2}, suggesting an inferior interference resistance of CF.

Catalytic stability is another critical parameter for nanostructured electrocatalysts. Our previous study revealed that the required anodic potential decreased with the increasing HMF concentration in a certain range [15]. In the presence of HMF, the anodic potential will rise as the reaction proceeds due to the gradual consumption of HMF, obstructing the observation of electrocatalytic stability of the electrode. To assess the durability of Co_3O_4/CF, four individual chronopotentiometric tests were executed at current densities of 10 mA cm^{-2}, 100 mA cm^{-2}, − 10 mA cm^{-2}, and − 100 mA cm^{-2} in the absence of HMF. As illustrated in Fig. 4c, after an adjustment within the initial 5 min, the anodic potentials required to reach 10 mA cm^{-2} and 100 mA cm^{-2} increased by less than 13 mV and 41 mV within 16 h, while the cathodic chronopotentiometry curves at − 10 mA cm^{-2} and − 100 mA cm^{-2}

Table 1
Comparison of electrocatalytic performance of bifunctional catalysts in 1 M KOH electrolyte.

Catalysts	HMF (M)	HMF oxidation potential (V vs. RHE)			HER overpotential (mV)		Ref.
		Onset	@ 10 mA cm^{-2}	@ 100 mA cm^{-2}	@ −10 mA·cm^{-2}	@ −100 mA·cm^{-2}	
Co_3O_4	0.01	0.945	1.079	1.400	177	294	This work
CoNW	0.01	0.886	1.311	1.764	232	~540	[15]
om-Co_3O_4	0.01	~1.3	1.39	NA	~170	NA	[17]
Ni_2P NPA	0.01	1.35	~1.36	~1.38	~160	NA	[25]
Co-P[a]	0.05	1.3	~1.36	NA	NA	NA	[24]
Ni_3S_2	0.01	~1.35	~1.36	~1.38	116	~225	[5]
hp-Ni	0.01	~1.35	~1.36	NA	181	~238	[12]
Ni_3N@C	0.01	1.35	~1.36	~1.4	~54	~150	[22]
NiSe@NiO_x	0.01	1.35	~1.35	~1.35	208	NA	[27]
Cu_xS@NiCo-LDH	0.01	1.18	~1.21	~1.31	107	~170	[40]
MoO_2-FeP@C	0.01	1.323	1.359	1.403	103	190	[41]
E-CoAl-LDH-NSA	0.01	1.3	NA	1.59	160	~390	[42]
N-MoO_2/Ni_3S_2	0.01	~1.34	~1.35	1.6	~200	300	[43]
Ni_3N-V_2O_3	0.01	~1.38	1.46	NA	53	~171	[23]

[a] the HER potentials were not given.

fluctuated within 8 mV and 12 mV, respectively. Such small potential variations manifest the robust durability of Co_3O_4/CF in the strong alkali environment.

To gain in-depth insight into the excellent catalytic performance of Co_3O_4/CF, intrinsic investigations were conducted by analyzing the vital electrochemical parameters. First, we compared the double-layer capacitance (C_{dl}) to estimate the electrochemically active surface area (ECSA), which follows the relationship of ECSA = C_{dl}/C_s, where the C_s is the specific capacitance and often described by an averaged unique value of 40 μF cm^{-2} for most electrode materials with a smooth and planar surface in 1 M alkaline electrolyte [44]. Cyclic voltammetry (CV) curves with different scan rates were acquired in the non-faradaic district of 0.625–0.725 V vs. RHE (Fig. S4). Accordingly, C_{dl} was determined from the slope of the linear regression between the current densities at 0.675 V vs. RHE and the scan rates. As presented in Fig. 4d, the C_{dl} of Co_3O_4/CF for OER is 18.3 mF cm^{-2}, five times that of CF (3.6 mF cm^{-2}), indicating that the surface of Co_3O_4/CF was much larger ECSA to expose more catalytically active sites [45]. Remarkably, with 10 mM HMF participation, the C_{dl} of Co_3O_4/CF and CF increased by 0.8 mF cm^{-2} and 0.2 mF cm^{-2}, respectively, indicating improved accessibility of charge carrier for HMF oxidation compared to OER and a more responsive Co_3O_4/CF over CF [20].

Resistance is an essential parameter to affect electrochemical performance. Accordingly, the electrochemical impedance spectroscopy (EIS) was measured to determine the solution resistance (R_s) and interfacial charge transfer resistance (R_{ct}). A relatively low potential of 1.6 V vs. RHE, slightly higher than the onset potential of Co foam without HMF, was chosen to ensure all the electrodes underwent the process of OER or HMF oxidation. As plotted in Fig. 4e, all the EIS spectra show a depressed semicircle with distinct diameters, indicating that OER and HMF oxidation processes occurred and were associated with charge transfer [46]. To obtain an acceptable fitting of the non-ideal semicircles, the constant phase element (CPE) was employed in place of the pure capacitor to construct the equivalent circuit. The optimum equivalent circuit and fit parameters compatible with the experimental measurement are presented in Fig. S5. Co_3O_4/CF and CF exhibit the very close R_s of 1.03–1.11 Ω in 1.0 M KOH, revealing that the growth of Co_3O_4 on the CF surface did not significantly affect the contact with the electrolyte. However, Co_3O_4/CF displays a small R_{ct} of only 0.48 Ω in 1.0 M KOH, much lower than the 3.66 Ω of CF, indicating the more rapid electron transport during OER process in contrast to the CF. After adding 10 mM HMF, the R_{ct} values for Co_3O_4/CF and CF were further reduced to 0.42 Ω and 3.39 Ω, respectively, confirming that the oxidation kinetics of HMF over both electrodes is better than that of OER. Due to the resistivity of an underlying compact oxide film, Co_3O_4/CF shows a higher electrode film resistance (R_{film}) of 0.65 Ω than that of CF (0.29 Ω), which is related to the inevitable surface passivation of metal Co. Anyhow, the sum of series resistance proves the superiority of Co_3O_4/CF over CF.

As the core concerns of electrocatalytic investigation, the selectivity to the target product and the energy utilization efficiency are well reflected in Faradaic efficiency (FE). Fig. 4f shows the FE of H_2 evolution and HMF oxidation over Co_3O_4/CF and the control CF. For HER, nearly unity FE was achieved on both Co_3O_4/CF and CF by chronoamperometry test at − 0.275 V vs. RHE, demonstrating that no possible reduction of organic molecules occurred at the cathode [47]. On the other hand, according to the parallel-consecutive reaction mechanism of HMF oxidation and the potential Cannizzaro reaction of the aldehyde group, several possible intermediates or uncertain byproducts are often generated and reduced the selectivity toward the desired FDCA, resulting in a low anodic FE. Despite the applied potential of 1.4 V vs. RHE far away from the onset potential for the competing oxygen evolution, the control sample of CF still received only a very low FE of 19.9% toward FDCA generation. The situation of Co_3O_4/CF is very different, with the corresponding value of 94.6% (Fig. S6), indicating the high selectivity to FDCA and energy efficiency over Co_3O_4/CF anode. Furthermore, the chronoampermetric time for passing the theoretically required charge of 29 C was 0.9 h and 8.0 h for Co_3O_4/CF and CF (Fig. S7), respectively, suggesting the designed electrode with a distinct advantage in respect of production efficiency for electrocatalytic oxidation.

3.3. Integrated evaluation in a two-electrode cell

The high activity and selectivity of Co_3O_4/CF, together with the two half-reactions' characteristics, inspired us to integrate FDCA production and H_2 generation in a membrane-free reactor to verify the superiority of coupling reactions with improving safety, maximizing energy utilization, and increasing productivity. Accordingly, two identical slices of Co_3O_4/CF were directly employed as anode and cathode to construct a two-electrode configuration with 5 mL electrolyte (1 M KOH) in the absence and presence of 10 mM HMF. As demonstrated in Fig. 5a, without the addition of HMF, the voltages required to achieve current densities of 10, 20, 50, and 100 mA cm^{-2} are 1.483 V, 1.693 V, 1.838 V, and 1.898 V, respectively, realizing the overall water splitting (OWS) over Co_3O_4/CF electrodes. This result is better than or equivalent to most of the reported catalysts for OWS at 10 mA cm^{-2}, such as Co_2P (1.65 V) [48], $NiCo_2O_4$ @ (Ni, Co)OOH (1.61 V) [49], NiFe@NC (1.81 V) [50], Cu_3P NB/Cu (1.85 V) [51], and C@Ni_8P_3 (1.65 V) [52]. When 10 mM HMF was presented, the corresponding voltages were further dropped to 1.385 V, 1.513 V, 1.641 V, and 1.737 V to reach the above representative current densities, reducing by 98–197 mV compared to OWS. Such results manifest that Co_3O_4/CF is of great potentiality in lowering the energy input of practical OWS. The participation of HMF further reduces the required voltage and generates

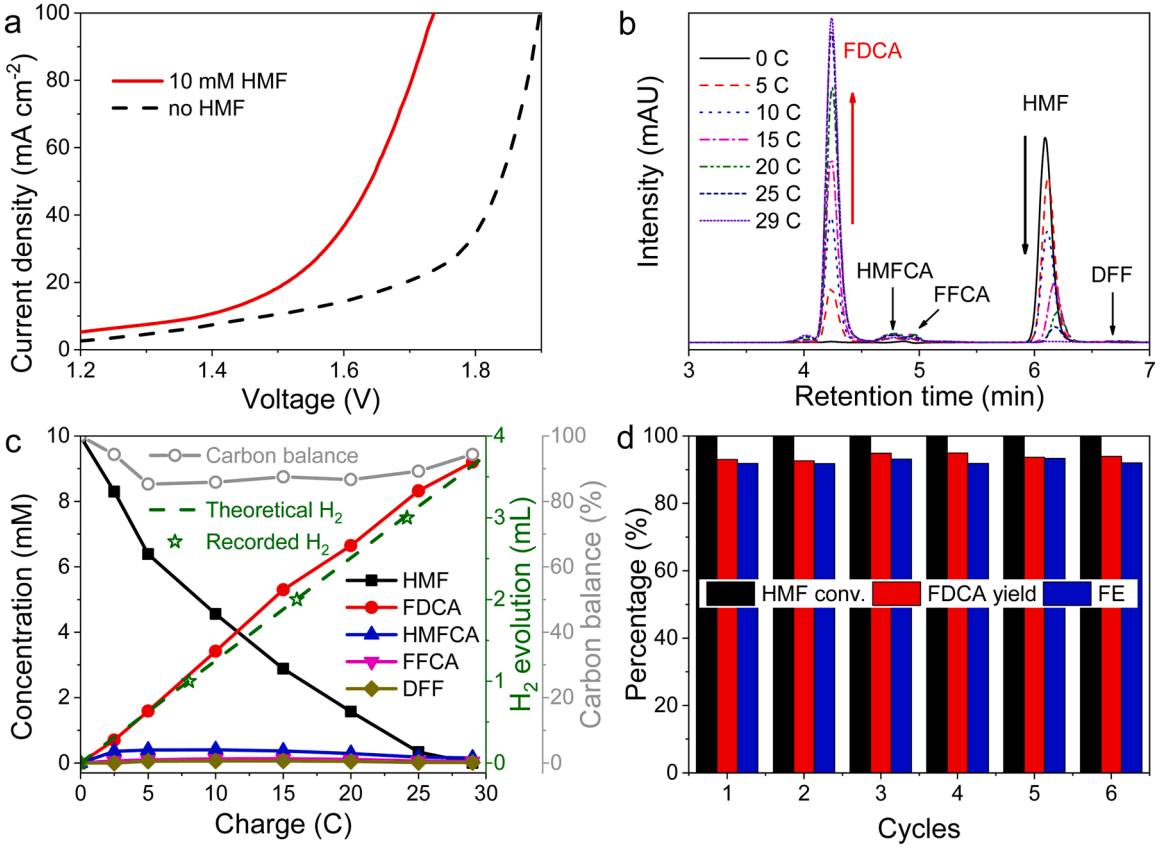

Fig. 5. Coupling reaction for simultaneous HMF oxidation and H_2 evolution in two-electrode system. (a) LSV curves in the absence and presence of 10 mM HMF. (b) HPLC chromatograms and (c) quantitative results of integration reaction at a voltage of 1.65 V. (d) Durability measurements.

products with higher values, suggesting the lowered reaction barrier and improved energy utilization efficiency by coupling strategy.

To quantitatively analyze the products of the integrated system, the chronoampermetric electrolysis was carried out at a constant voltage of 1.65 V to input the theoretical charge of 29 C. At this voltage, bubbles were only generated at the cathode, and the volume of escaped H_2 matched the theoretical ones very well (Fig. 5c). Besides, the purity of H_2 determined by GC detection is almost 100% (Fig. S8), suggesting hydrogen as the unique released gas in the system. HPLC plots and the relative quantitative analysis of the liquid phase are shown in Fig. 5b&c. During the whole course of electrolysis, the peak of FDCA rose gradually with the declining HMF signal, accompanied by two tiny peaks assigned to HMFCA and FFCA but no detectable DFF signal. Thus, the HMF oxidation was inferred to undergo the HMFCA pathway (HMF → HMFCA → FFCA → FDCA), agreeing with our previous studies and most of the researches in basic solutions [53]. As the passing charge increases, HMF selectively converted into FDCA, eventually achieving 100% conversion with 93.2% yield and 92.9% FE within 0.86 h. The results prove that the HMF oxidation reaction successfully substituted OER and consequently realized the coupling of biomass value-added reactions with HER. The carbon balance varied from 100% to 85.3% during the electrolysis and finally achieved 94.4%, suggesting that the majority of the undetectable intermediates and adsorbed organics can ultimately convert to FDCA. The production rates for H_2 and FDCA were calculated to be 0.175 mmol h^{-1} and 0.054 mmol h^{-1}, respectively. Notably, as depicted in Fig. 5d, Co_3O_4/CF always preserved good catalytic performance with 100~99.9% HMF conversion, 95.0~92.7% FDCA yield, and 93.3~91.8% FE in six successive electrolysis. Although a low concentration of Co (0.059 ± 0.005 mg L^{-1}) was detected in the post-electrolyte by the ICP-OES detection, the hydrangea-like morphology, crystal structure, and crystallinity were maintained very well (Fig. 6&S9), illustrating the leaching of Co has a negligible effect on the performance and structural durability of Co_3O_4/CF.

3.4. Electrocatalytic oxidation of BHMF, FFA, FF, and DFF

The highly selective electro-oxidation of aldehyde and hydroxyl groups rather than destruction of the furan ring encouraged us to search for more candidates to harvest the value-added FDCA. Compared to the hydroxyl group, the unstable aldehyde group often induces the instability of HMF to form humins [54], which are dark-colored insoluble and seriously affect the purity of the final FDCA product. By replacing aldehyde with hydroxyl to increase the storage stability and product purity, BHMF was employed as an alternative to HMF to simultaneously produce FDCA and H_2 in a two-electrode configuration (Fig. 7a). When 10 mM BHMF was used in the same setup with two identical Co_3O_4/CF electrodes, the voltages required to reach current densities of 20, 50, and 100 mA cm^{-2} were significantly reduced by 121, 156, and 56 mV compared to OWS (Fig. 7b), respectively, verifying BHMF containing double hydroxyl groups as a desirable candidate. Due to the more stable molecular structure (Fig. S10) [55], the voltage required to oxidize BHMF was slightly higher than that for HMF oxidation. In addition, since the overall conversion of BHMF to FDCA is an eight-electron process, ~38.6 C theoretical amount of charge is required to perfectly convert 5 mL BHMF (10 mM) into FDCA. As depicted in Fig. 7c, after chronoamperometry at 1.65 V for 1.67 h, the integrated reaction received a 100% BHMF conversion with a 95.82% yield and 95.79% FE toward FDCA. During the whole electrolysis, bubbles escaped only from the cathode. The gas volumes recorded at different amounts of charge were in good agreement with the theoretically calculated H_2 values with a final FE of 96.1%, slightly lower than that of the coupled HMF electrolysis. The carbon balance smoothly ran and was consistently above

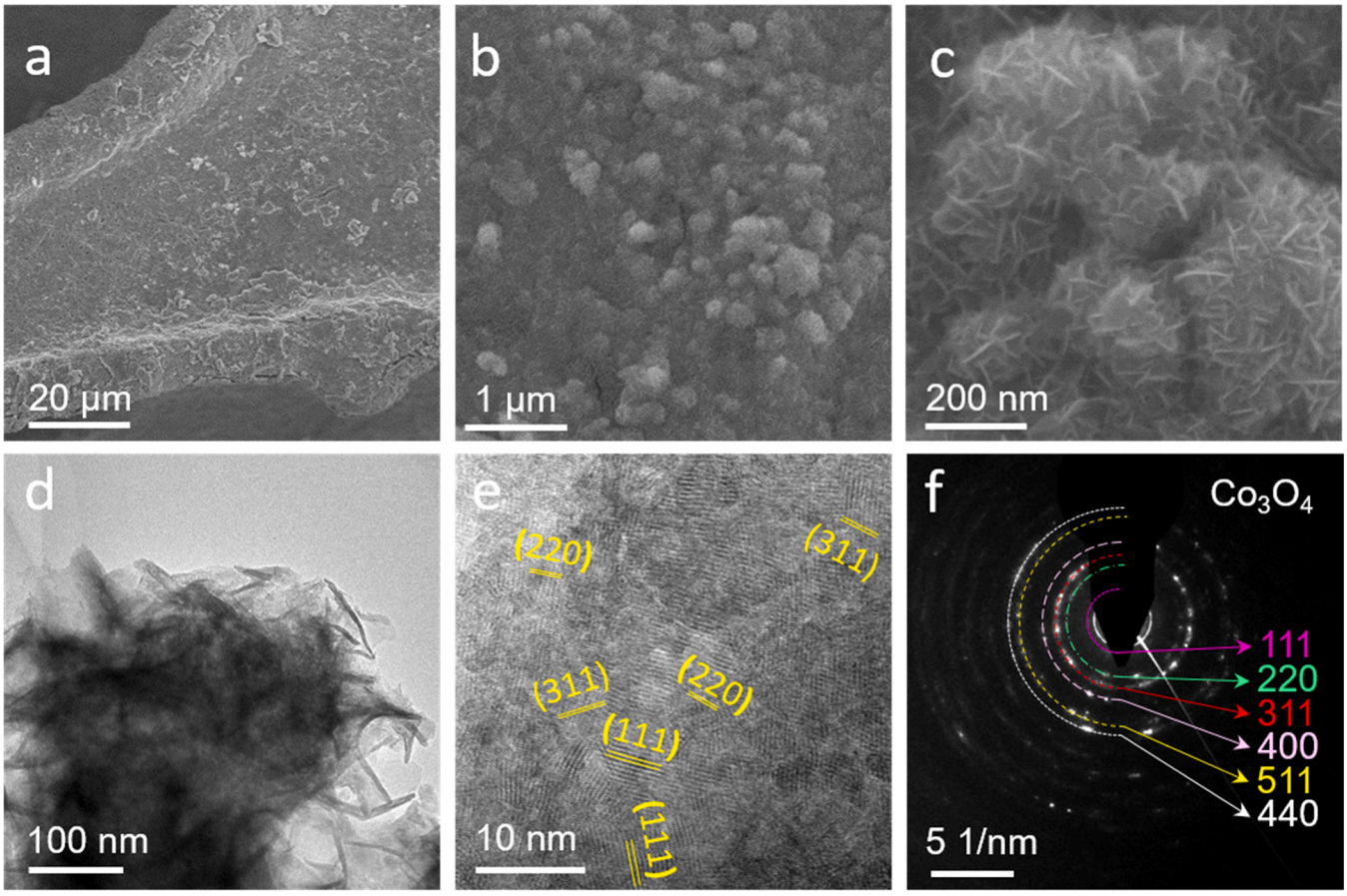

Fig. 6. Characterization of Co_3O_4/CF electrode after six successive electrolysis. (a-c) SEM images. (d-e) TEM images and (f) SAED pattern of exfoliated Co_3O_4.

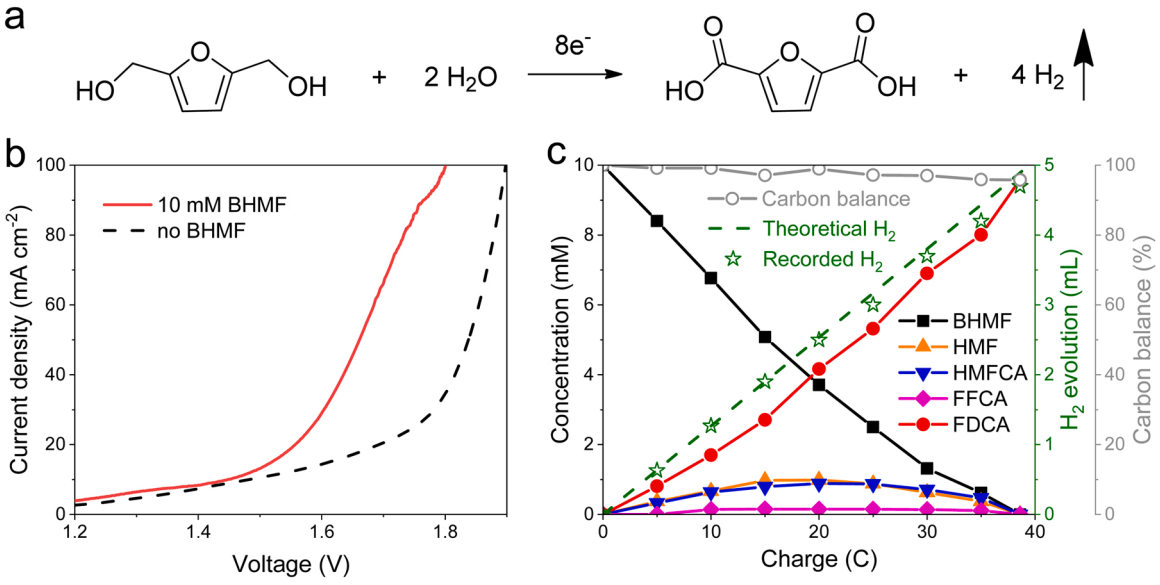

Fig. 7. BHMF as a substrate for coupling reaction in two-electrode system. (a) Overall reaction formula for BHMF electrolysis with H_2O to generate FDCA and H_2. (b) LSV curves in the absence and presence of 10 mM BHMF. (c) HPLC quantitative results and H_2 evolution of integration reaction.

95.8%, superior to the situation of HMF electrolysis with sharp decline and rise ones (Fig. 5c). Besides, the high universality of Co_3O_4/CF for upgrading biomass was demonstrated by using other representative substituent-containing furans, FFA, FF, and DFF, as the oxidation substrates, dramatically reducing the potential required or increasing the current densities (Fig. 8).

3.5. PVEC integration reaction under outdoor sunshine

Solar energy, the ultimate source of most energy on the planet,

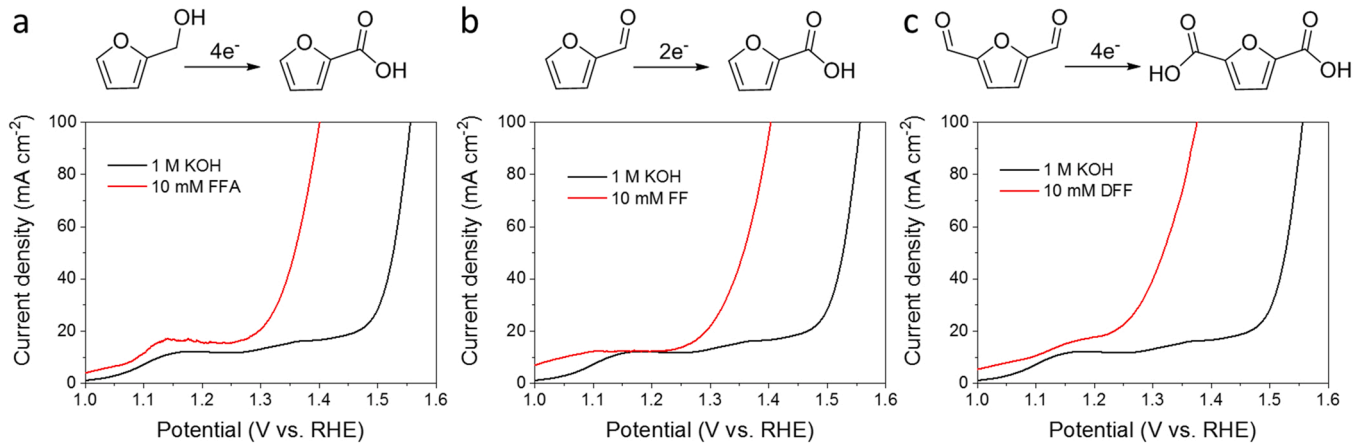

Fig. 8. Electrocatalytic oxidation of other substituent-containing furans. (a) FFA, (b) FF, (c) DFF.

introduced to the catalytic reactions can dramatically shorten the energy utilization path and improve the overall sustainability. In photocatalysis (PC)[56] and photoelectrocatalysis (PEC)[57], the oxidation ability of photogenerated holes is determined by the valence-band position of catalysts. For HMF oxidation, it is challenging to fabricate appropriate bandgap structures to selective yield FDCA rather than destroy the furan ring till mineralize to CO_2. To overcome this limitation, 2,2,6,6-tetramethylpiperidine-1-oxyl (TEMPO) is often added to PEC to oxidize HMF selectively. However, the homogeneous TEMPO increased the production cost and isolation difficulty. A recent review has pointed out that the solar-to-hydrogen efficiency of PVEC is nearly an order of magnitude higher than that of the PEC [58]. Therefore, we employ PVEC under natural sunlight irradiation to verify the efficient production of FDCA and hydrogen from solar energy. As illustrated in Fig. 9a, the PVEC were coupled by photovoltaic (PV) and electrochemical (EC) parts in the most straightforward way. A 0.65 W commercial solar cell battery was employed to provide a roughly stable voltage of 1.60 ± 0.02 V by adjusting the light shade (Fig. 9b). The electrolysis cell contained two identical Co_3O_4/CF electrodes with 5 mL KOH electrolyte and 10.4 mM BHMF. As recorded in Fig. 9c, BHMF was consumed entirely within 90 min, while the yield of FDCA increased accordingly to 93.5% with small amounts of HMF and HMFCA as transient intermediates during

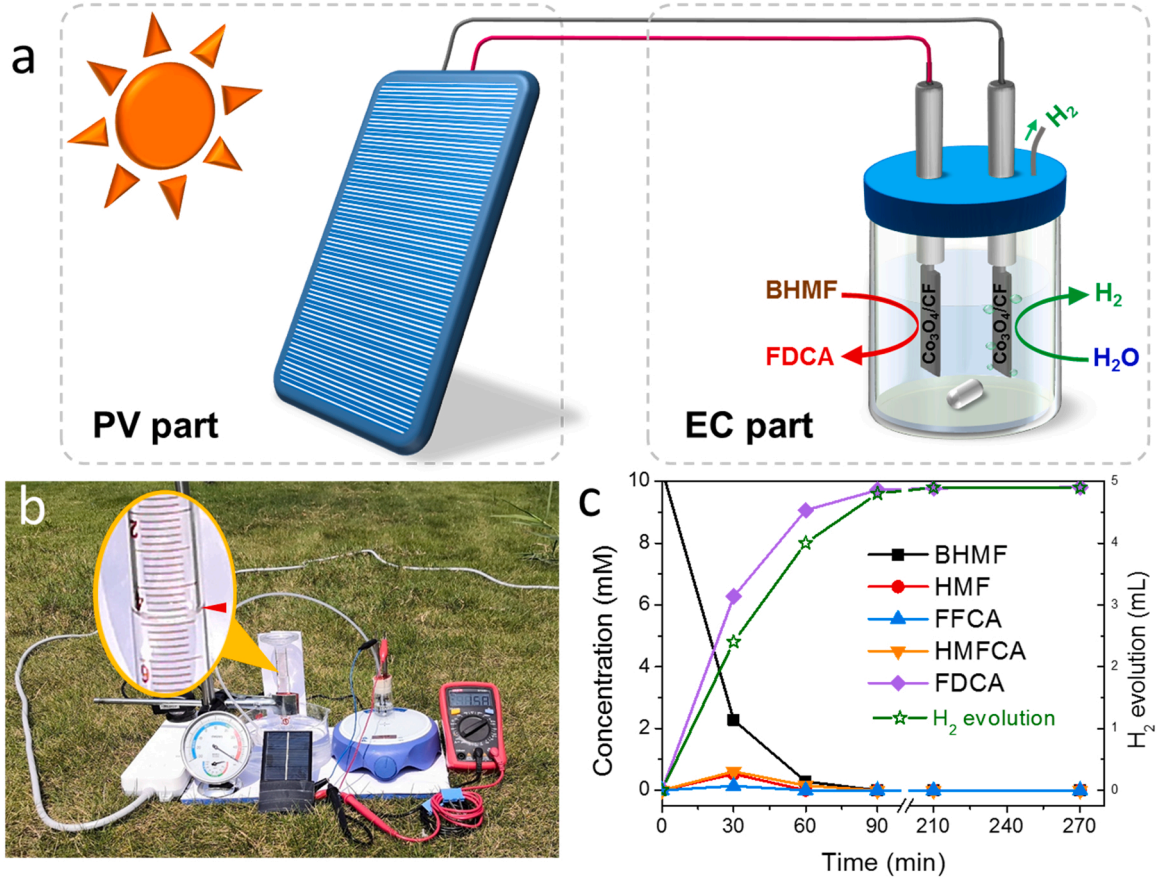

Fig. 9. PVEC for simultaneous BHMF oxidation and HER. (a) Schematic illustration. (b) Photographic image at 90 min under natural sunlight irradiation in Ningbo. (c) Time-course of BHMF oxidation and HER.

oxidation. Hydrogen was generated synchronously with FDCA and reached a volume of 4.8 mL in 90 min (Fig. S11), which is highly consistent with the theoretical value (4.72 mL) according to the reaction formula in Fig. 7a. As the illumination time extended to 270 min, FDCA yield and H_2 volume increased by only 0.9% and 0.1 mL, respectively. This indicated that adding BHMF into PVEC not only harvested the value-added FDCA but also significantly sped up hydrogen production, thus greatly improving the solar energy utilization efficiency.

4. Conclusions

In summary, a hydrangea-like Co_3O_4 catalyst was established on cobalt foam by in-situ electrochemical tuning nonporous CoS_x as a highly effective versatile electrocatalyst for membrane-free hydrogen evolution and furan upgrading. The defective structure endows Co_3O_4/CF with high electrochemical activity, requiring an operating voltage of only 1.385 V to accomplish the simultaneous HMF oxidation and H_2 evolution at 10 mA cm^{-2} current density in an integration electrolyzer. After injecting the theoretical amount of charge (29 C) at a constant voltage of 1.65 V, HMF was fully converted with 93.2% yield and 92.9% FE toward FDCA, while pure hydrogen was released efficiently at a rate of 0.175 mmol h^{-1} from the coupling system with 99.8% FE. In addition, Co_3O_4/CF exhibited excellent catalytic durability without obvious structural destroy after six successive electrolysis. The high universality of catalyst was also validated by oxidizing other representative furans, such as BHMF, FFA, FF, and DFF, all realizing a dramatic reduction in required potential compared to pure OER. Especially, BHMF electrooxidation over Co_3O_4/CF acquired a more desirable performance with 95.82% yield and 95.79% FE, highlighting BHMF as a novel and superior feedstock to develop downstream derivatives due to its higher thermal and chemical stability. Coupling a commercial solar cell with a symmetric membrane-free electrolyzer in parallel realized the efficient production of FDCA and hydrogen under natural sunlight irradiation, that demonstrated the promising prospect of PVEC for biomass valorization and green energy production.

CRediT authorship contribution statement

J.Z. supervised the project. C.L.C. led the overall work, proposed the experimental design, and rewrote the manuscript. Z.Q.Z. performed the partial synthesis, characterization, electrochemical testing, as well as initial draft preparation. J.L. and B.Z. supplemented the critical structural identification, reaction data, and PVEC experiments. H.L.H., Y.Y., G.X.C., and M.R.G. participated in the technical discussion. All authors have approved the final version of the manuscript.

Declaration of Competing Interest

The authors declare that they have no known competing financial interests or personal relationships that could have appeared to influence the work reported in this paper.

Acknowledgments

The authors gratefully acknowledge the technical and writing assistance from Haitao Yu (Nimte, CAS), Prof. Shuchang Wu (Taizhou University) and Prof. Soliman El-Hout (CMRDI, Egypt), as well as the financial support from the National Natural Science Foundation of China (22072170), Zhejiang Provincial Natural Science Foundation of China (LY19B030003, LQ19B060002), Key Research and Development Program of Zhejiang Province (2021C03170), Ningbo Science and Technology Bureau (2018B10056, 2019B10096), and Chinese Academy of Sciences (QYZDB-SSW-JSC037).

Appendix A. Supporting information

Supplementary data associated with this article can be found in the online version at doi:10.1016/j.apcatb.2022.121209.

References

[1] M. Carmo, D.L. Fritz, J. Merge, D. Stolten, A comprehensive review on PEM water electrolysis, Int. J. Hydrog. Energy 38 (2013) 4901–4934, https://doi.org/10.1016/j.ijhydene.2013.01.151.
[2] C. Tang, Y. Zheng, M. Jaroniec, S.Z. Qiao, Electrocatalytic refinery for sustainable production of fuels and chemicals, Angew. Chem. Int Ed. 60 (2021) 19572–19590, https://doi.org/10.1002/anie.202101522.
[3] K. Li, Y.J. Sun, Electrocatalytic upgrading of biomass-derived intermediate compounds to value-added products, Chem. -Eur. J. 24 (2018) 18258–18270, https://doi.org/10.1002/chem.201803319.
[4] C. Xu, E. Paone, D. Rodriguez-Padron, R. Luque, F. Mauriello, Recent catalytic routes for the preparation and the upgrading of biomass derived furfural and 5-hydroxymethylfurfural, Chem. Soc. Rev. 49 (2020) 4273–4306, https://doi.org/10.1039/d0cs00041h.
[5] B. You, X. Liu, N. Jiang, Y.J. Sun, A general strategy for decoupled hydrogen production from water splitting by integrating oxidative biomass valorization, J. Am. Chem. Soc. 138 (2016) 13639–13646, https://doi.org/10.1021/jacs.6b07127.
[6] K.R. Vuyyuru, P. Strasser, Oxidation of biomass derived 5-hydroxymethylfurfural using heterogeneous and electrochemical catalysis, Catal. Today 195 (2012) 144–154, https://doi.org/10.1016/j.cattod.2012.05.008.
[7] P. Parpot, A.P. Bettencourt, G. Chamoulaud, K.B. Kokoh, E.M. Beigsir, Electrochemical investigations of the oxidation-reduction of furfural in aqueous medium - application to electrosynthesis, Electrochim. Acta 49 (2004) 397–403, https://doi.org/10.1016/j.electacta.2003.08.021.
[8] C.M. Zhou, W.R. Shi, X.Y. Wan, Y. Meng, Y. Yao, Z. Guo, Y.H. Dai, C. Wang, Y. H. Yang, Oxidation of 5-hydroxymethylfurfural over a magnetic iron oxide decorated rGO supporting Pt nanocatalyst, Catal. Today 330 (2019) 92–100, https://doi.org/10.1016/j.cattod.2018.05.037.
[9] Y.X. Lu, T.Y. Liu, C.L. Dong, Y.C. Huang, Y.F. Li, J. Chen, Y.Q. Zou, S.Y. Wang, Tuning the selective adsorption site of biomass on Co_3O_4 by Ir single atoms for electrosynthesis, Adv. Mater. 33 (2021), 2007056, https://doi.org/10.1002/adma.202007056.
[10] D.J. Chadderdon, L. Xin, J. Qi, Y. Qiu, P. Krishna, K.L. More, W.Z. Li, Electrocatalytic oxidation of 5-hydroxymethylfurfural to 2,5-furandicarboxylic acid on supported Au and Pd bimetallic nanoparticles, Green Chem. 16 (2014) 3778–3786, https://doi.org/10.1039/c4gc00401a.
[11] X.Y. Lu, K.H. Wu, B.S. Zhang, J.N. Chen, F. Li, B.J. Su, P.Q. Yan, J.M. Chen, W. Qi, Highly efficient electro-reforming of 5-hydroxymethylfurfural on vertically oriented nickel nanosheet/carbon hybrid catalysts: structure-function relationships, Angew. Chem. Int. Ed. 60 (2021) 14528–14535, https://doi.org/10.1002/anie.202102359.
[12] B. You, X. Liu, X. Liu, Y.J. Sun, Efficient H_2 evolution coupled with oxidative refining of alcohols via a hierarchically porous nickel bifunctional electrocatalyst, ACS Catal. 7 (2017) 4564–4570, https://doi.org/10.1021/acscatal.7b00876.
[13] B. Mondal, N. Karjule, C. Singh, R. Shimoni, M. Volokh, I. Hod, M. Shalom, Unraveling the mechanisms of electrocatalytic oxygenation and dehydrogenation of organic molecules to value-added chemicals over a Ni-Fe oxide catalyst, Adv. Energy Mater. 11 (2021), 2101858, https://doi.org/10.1002/aenm.202101858.
[14] K.Z. Gu, D.D. Wang, C. Xie, T.H. Wang, G. Huang, Y.B. Liu, Y.Q. Zou, L. Tao, S. Y. Wang, Defect-rich high-entropy oxide nanosheets for efficient 5-hydroxymethylfurfural electrooxidation, Angew. Chem. Int. Ed. 60 (2021) 20253–20258, https://doi.org/10.1002/anie.202107390.
[15] Z.Q. Zhou, C.L. Chen, M.R. Gao, B.W. Xia, J. Zhang, In situ anchoring of a Co_3O_4 nanowire on nickel foam: an outstanding bifunctional catalyst for energy-saving simultaneous reactions, Green Chem. 21 (2019) 6699–6706, https://doi.org/10.1039/c9gc02880c.
[16] M.J. Kang, H. Park, J. Jegal, S.Y. Hwang, Y.S. Kang, H.G. Cha, Electrocatalysis of 5-hydroxymethylfurfural at cobalt based spinel catalysts with filamentous nanoarchitecture in alkaline media, Appl. Catal. B 242 (2019) 85–91, https://doi.org/10.1016/j.apcatb.2018.09.087.
[17] C.L. Wang, H.J. Bongard, M.Q. Yu, F. Schuth, Highly ordered mesoporous Co_3O_4 electrocatalyst for efficient, selective, and stable oxidation of 5-hydroxymethylfurfural to 2,5-furandicarboxylic acid, ChemSusChem 14 (2021) 5199–5206, https://doi.org/10.1002/cssc.202002762.
[18] X.H. Deng, G.Y. Xu, Y.J. Zhang, L. Wang, J.J. Zhang, J.F. Li, X.Z. Fu, J.L. Luo, Understanding the roles of electrogenerated Co^{3+} and Co^{4+} in selectivity-tuned 5-hydroxymethylfurfural oxidation, Angew. Chem. Int. Ed. 60 (2021) 20535–20542, https://doi.org/10.1002/anie.202108955.
[19] G. Grabowski, J. Lewkowski, R. Skowronski, The electrochemical oxidation of 5-hydroxymethylfurfural with the nickel-oxide hydroxide electrode, Electrochim. Acta 36 (1991) 1995, https://doi.org/10.1016/0013-4686(91)85084-K.
[20] W.J. Liu, L.N. Dang, Z.R. Xu, H.Q. Yu, S. Jin, G.W. Huber, Electrochemical oxidation of 5-hydroxymethylfurfural with nife layered double hydroxide (LDH) nanosheet catalysts, ACS Catal. 8 (2018) 5533–5541, https://doi.org/10.1021/acscatal.8b01017.
[21] H. Chen, J.T. Wang, Y. Yao, Z.H. Zhang, Z.Z. Yang, J. Li, K.Q. Chen, X.Y. Lu, P. K. Ouyang, J. Fu, Cu-Ni bimetallic hydroxide catalyst for efficient electrochemical

conversion of 5-hydroxymethylfurfural to 2,5-furandicarboxylic acid, ChemElectroChem 6 (2019) 5797–5801, https://doi.org/10.1002/celc.201901366.
[22] N.N. Zhang, Y.Q. Zou, L. Tao, W. Chen, L. Zhou, Z.J. Liu, B. Zhou, G. Huang, H. Z. Lin, S.Y. Wang, Electrochemical oxidation of 5-hydroxymethylfurfural on nickel nitride/carbon nanosheets: reaction pathway determined by in situ sum frequency generation vibrational spectroscopy, Angew. Chem. Int. Ed. 58 (2019) 15895–15903, https://doi.org/10.1002/anie.201908722.
[23] S.Q. Liang, L.H. Pan, T. Thomas, B. Zhu, C.L. Chen, J. Zhang, H.J. Shen, J. Liu, M. H. Yang, Ni_3N-V_2O_3 enables highly efficient 5-(Hydroxymethyl) furfural oxidation enabling membrane free hydrogen production, Chem. Eng. J. 415 (2021), 128864, https://doi.org/10.1016/j.cej.2021.128864.
[24] N. Jiang, B. You, R. Boonstra, I.M.T. Rodriguez, Y.J. Sun, Integrating electrocatalytic 5-hydroxymethylfurfural oxidation and hydrogen production via Co-P-derived electrocatalysts, ACS Energy Lett. 1 (2016) 386–390, https://doi.org/10.1021/acsenergylett.6b00214.
[25] B. You, N. Jiang, X. Liu, Y.J. Sun, Simultaneous H_2 generation and biomass upgrading in water by an efficient noble-metal-free bifunctional electrocatalyst, Angew. Chem. Int. Ed. 55 (2016) 9913–9917, https://doi.org/10.1002/anie.201603798.
[26] P.L. Zhang, X. Sheng, X.Y. Chen, Z.Y. Fang, J. Jiang, M. Wang, F.S. Li, L.Z. Fan, Y. S. Ren, B.B. Zhang, B.J.J. Timmer, M.S.G. Ahlquist, L.C. Sun, Paired electrocatalytic oxygenation and hydrogenation of organic substrates with water as the oxygen and hydrogen source, Angew. Chem. Int. Ed. 58 (2019) 9155–9159, https://doi.org/10.1002/anie.201903936.
[27] L.F. Gao, Z.B. Liu, J.L. Ma, L.J. Zhong, Z.Q. Song, J.A. Xu, S.Y. Gan, D.X. Han, L. Niu, NiSe@NiOx core-shell nanowires as a non-precious electrocatalyst for upgrading 5-hydroxymethylfurfural into 2,5-furandicarboxylic acid, Appl. Catal. B 261 (2020), 118235, https://doi.org/10.1016/j.apcatb.2019.118235.
[28] Y. Zhong, R.Q. Ren, J.B. Wang, Y.Y. Peng, Q. Li, Y.M. Fan, Grass-like NixSey nanowire arrays shelled with NiFe LDH nanosheets as a 3D hierarchical core-shell electrocatalyst for efficient upgrading of biomass-derived 5-hydroxymethylfurfural and furfural, Catal. Sci. Technol. 12 (2021) 201–211, https://doi.org/10.1039/D1CY01816G.
[29] R.J. Lin, T.X. Lin, J.Y. Huang, X.H. Huang, Y.J. Liu, Hierarchical cobalt sulfide with vertical in-plane edge structure for enhanced electrocatalytic oxygen evolution reaction, Electrochim. Acta 281 (2018) 348–356, https://doi.org/10.1016/j.electacta.2018.05.184.
[30] X.H. Xia, C.R. Zhu, J.S. Luo, Z.Y. Zeng, C. Guan, C.F. Ng, H. Zhang, H.J. Fan, Synthesis of free-standing metal sulfide nanoarrays via anion exchange reaction and their electrochemical energy storage application, Small 10 (2014) 766–773, https://doi.org/10.1002/smll.201302224.
[31] Y.X. Lu, C.L. Dong, Y.C. Huang, Y.Q. Zou, Z.J. Liu, Y.B. Liu, Y.Y. Li, N.H. He, J. Q. Shi, S.Y. Wang, Identifying the geometric site dependence of spinel oxides for the electrooxidation of 5-hydroxymethylfurfural, Angew. Chem. Int. Ed. 59 (2020) 19215–19221, https://doi.org/10.1002/anie.202007767.
[32] J.S. Luo, J.H. Im, M.T. Mayer, M. Schreier, M.K. Nazeeruddin, N.G. Park, S. D. Tilley, H.J. Fan, M. Gratzel, Water photolysis at 12.3% efficiency via perovskite photovoltaics and Earth-abundant catalysts, Science 345 (2014) 1593–1596, https://doi.org/10.1126/science.1258307.
[33] L.L. Feng, G.T. Yu, Y.Y. Wu, G.D. Li, H. Li, Y.H. Sun, T. Asefa, W. Chen, X.X. Zou, High-index faceted Ni_3S_2 nanosheet arrays as highly active and ultrastable electrocatalysts for water splitting, J. Am. Chem. Soc. 137 (2015) 14023–14026, https://doi.org/10.1021/jacs.5b08186.
[34] H.Y. Jin, J. Wang, D.F. Su, Z.Z. Wei, Z.F. Pang, Y. Wang, In situ cobalt-cobalt oxide/N-doped carbon hybrids as superior bifunctional electrocatalysts for hydrogen and oxygen evolution, J. Am. Chem. Soc. 137 (2015) 2688–2694, https://doi.org/10.1021/ja5127165.
[35] H.B. Zhang, Z.J. Ma, J.J. Duan, H.M. Liu, G.G. Liu, T. Wang, K. Chang, M. Li, L. Shi, X.G. Meng, K.C. Wu, J.H. Ye, Active sites implanted carbon cages in core shell architecture: highly active and durable electrocatalyst for hydrogen evolution reaction, ACS Nano 10 (2016) 684–694, https://doi.org/10.1021/acsnano.5b05728.
[36] Q. Zhang, C.C. Zhang, J.B. Liang, P.G. Yin, Y. Tian, Orthorhombic α-NiOOH nanosheet arrays: phase conversion and efficient bifunctional electrocatalysts for full water splitting, ACS Sustain. Chem. Eng. 5 (2017) 3808–3818, https://doi.org/10.1021/acssuschemeng.6b02788.
[37] K.S. Bhat, H.S. Nagaraja, Nickel selenide nanostructures as an electrocatalyst for hydrogen evolution reaction, Int. J. Hydrog. Energy 43 (2018) 19851–19863, https://doi.org/10.1016/j.ijhydene.2018.09.018.
[38] P. Guo, J. Wu, X.B. Li, J. Luo, W.M. Lau, H. Liu, X.L. Sun, L.M. Liu, A highly stable bifunctional catalyst based on 3D Co(OH)(2)@NCNTs@NF towards overall water-splitting, Nano Energy 47 (2018) 96–104, https://doi.org/10.1016/j.nanoen.2018.02.032.
[39] H.L. Li, W.Y. Yuan, Q. Wang, X. Cui, J. Jiang, S.M. Chen, L. Song, X.H. Guo, Two-dimensional cobalt oxy-hydrate sulfide nanosheets with modified t(2g) orbital state of CoO6-x octahedron for efficient overall water splitting, ACS Sustain. Chem. Eng. 7 (2019) 17325–17334, https://doi.org/10.1021/acssuschemeng.9b04256.
[40] X.H. Deng, X.M. Kang, M. Li, K. Xiang, C. Wang, Z.P. Guo, J.J. Zhang, X.Z. Fu, J. L. Luo, Coupling efficient biomass upgrading with H_2 production via bifunctional Cu_xS@NiCo-LDH core-shell nanoarray electrocatalysts, J. Mater. Chem. A 8 (2020) 1138–1146, https://doi.org/10.1039/c9ta06917h.
[41] G.C. Yang, Y.Q. Jiao, H.J. Yan, Y. Xie, A.P. Wu, X. Dong, D.Z. Guo, C.G. Tian, H. G. Fu, Interfacial engineering of MoO_2-FeP heterojunction for highly efficient hydrogen evolution coupled with biomass electrooxidation, Adv. Mater. 32 (2020), 2000455, https://doi.org/10.1002/adma.202000455.
[42] Y.J. Song, Z.H. Li, K. Fan, Z. Ren, W.F. Xie, Y.S. Yang, M.F. Shao, M. Wei, Ultrathin layered double hydroxides nanosheets array towards efficient electrooxidation of 5-hydroxymethylfurfural coupled with hydrogen generation, Appl. Catal. B 299 (2021), 120669, https://doi.org/10.1016/j.apcatb.2021.120669.
[43] L. Wang, J.H. Cao, C.J. Lei, Q.Z. Dai, B. Yang, Z.J. Li, X.W. Zhang, C. Yuan, L.C. Lei, Y. Hou, Strongly coupled 3D N-doped MoO_2/Ni_3S_2 hybrid for high current density hydrogen evolution electrocatalysis and biomass upgrading, ACS Appl. Mater. Interfaces 11 (2019) 27743–27750, https://doi.org/10.1021/acsami.9b06502.
[44] C.C.L. McCrory, S.H. Jung, J.C. Peters, T.F. Jaramillo, Benchmarking heterogeneous electrocatalysts for the oxygen evolution reaction, J. Am. Chem. Soc. 135 (2013) 16977–16987, https://doi.org/10.1021/ja407115p.
[45] H. Liu, F.X. Ma, C.Y. Xu, L. Yang, Y. Du, P.P. Wang, S. Yang, L. Zhen, Sulfurizing-induced hollowing of Co_9S_8 microplates with nanosheet units for highly efficient water oxidation, ACS Appl. Mater. Interfaces 9 (2017) 11634–11641, https://doi.org/10.1021/acsami.7b00899.
[46] C. Chang, L. Zhang, C.W. Hsu, X.F. Chuah, S.Y. Lu, Mixed NiO/$NiCo_2O_4$ nanocrystals grown from the skeleton of a 3D porous nickel network as efficient electrocatalysts for oxygen evolution reactions, ACS Appl. Mater. Interfaces 10 (2018) 417–426, https://doi.org/10.1021/acsami.7b13127.
[47] Y. Kwon, K.J.P. Schouten, J.C. van der Waal, E. de Jong, M.T.M. Koper, Electrocatalytic conversion of furanic compounds, ACS Catal. 6 (2016) 6704–6717, https://doi.org/10.1021/acscatal.6b01861.
[48] M.J. Song, Y. He, M.M. Zhang, X.R. Zheng, Y. Wang, J.F. Zhang, X.P. Han, C. Zhong, W.B. Hu, Y.D. Deng, Controllable synthesis of Co_2P nanorods as high-efficiency bifunctional electrocatalyst for overall water splitting, J. Power Sources 402 (2018) 345–352, https://doi.org/10.1016/j.jpowsour.2018.09.042.
[49] L.M. Tao, M. Li, S.H. Wu, Q.L. Wang, X. Xiao, Q.W. Li, M.K. Wang, Y.Q. Fu, Y. Shen, Sea coral-like $NiCo_2O_4$@(Ni, Co)OOH heterojunctions for enhancing overall watersplitting, Catal. Sci. Technol. 8 (2018) 4151–4158, https://doi.org/10.1039/c8cy00624e.
[50] Z.P. Zhang, Y.S. Qin, M.L. Dou, J. Ji, F. Wang, One-step conversion from Ni/Fe polyphthalocyanine to N-doped carbon supported Ni-Fe nanoparticles for highly efficient water splitting, Nano Energy 30 (2016) 426–433, https://doi.org/10.1016/j.nanoen.2016.10.035.
[51] S.T. Wei, K. Qi, Z. Jin, J.S. Cao, W.T. Zheng, H. Chen, X.Q. Cui, One-step synthesis of a self-supported copper phosphide nanobush for overall water splitting, ACS Omega 1 (2016) 1367–1373, https://doi.org/10.1021/acsomega.6b00366.
[52] J. Yu, Q.Q. Li, N. Chen, C.Y. Xu, L. Zhen, J.S. Wu, V.P. Dravid, Carbon-coated nickel phosphide nanosheets as efficient dual-electrocatalyst for overall water splitting, ACS Appl. Mater. Interfaces 8 (2016) 27850–27858, https://doi.org/10.1021/acsami.6b10552.
[53] C.L. Chen, L.C. Wang, B. Zhu, Z.Q. Zhou, S.I. El-Hout, J. Yang, J. Zhang, 2,5-Furandicarboxylic acid production via catalytic oxidation of 5-hydroxymethylfurfural: catalysts, processes and reaction mechanism, J. Energy Chem. 54 (2021) 528–554, https://doi.org/10.1016/j.jechem.2020.05.068.
[54] G. Tsilomelekis, T.R. Josephson, V. Nikolakis, S. Caratzoulas, Origin of 5-hydroxymethylfurfural stability in water/dimethyl sulfoxide mixtures, ChemSusChem 7 (2014) 117–126, https://doi.org/10.1002/cssc.201300786.
[55] B. Zhu, C.L. Chen, L.Y. Huai, Z.Q. Zhou, L. Wang, J. Zhang, 2,5-Bis(hydroxymethyl) furan: a new alternative to HMF for simultaneously electrocatalytic production of FDCA and H_2 over CoOOH/Ni electrodes, Appl. Catal. B 297 (2021), 120396, https://doi.org/10.1016/j.apcatb.2021.120396.
[56] G.Q. Han, Y.H. Jin, R.A. Burgess, N.E. Dickenson, X.M. Cao, Y.J. Sun, Visible-light-driven valorization of biomass intermediates integrated with H_2 production catalyzed by ultrathin Ni/CdS nanosheets, J. Am. Chem. Soc. 139 (2017) 15584–15587, https://doi.org/10.1021/jacs.7b08657.
[57] H.G. Cha, K.S. Choi, Combined biomass valorization and hydrogen production in a photoelectrochemical cell, Nat. Chem. 7 (2015) 328–333, https://doi.org/10.1038/Nchem.2194.
[58] Z. Wang, Y. Gu, L. Wang, Revisiting solar hydrogen production through photovoltaic-electrocatalytic and photoelectrochemical water splitting, Front. Energy 15 (2021) 596–599, https://doi.org/10.1007/s11708-021-0745-0.